A Split-Coefficient/Locally Monotonic Scheme for Multishocked Supersonic Flow

James E. Daywitt* and David J. Szostowski†
General Electric Company, Philadelphia, Pennsylvania
and
Dale A. Anderson‡
Iowa State University, Ames, Iowa

A new finite-difference technique is developed for solving three-dimensional, steady, inviscid, supersonic, equilibrium real-gas flows with embedded shock waves. The technique employs the split-coefficient matrix (SCM) method to solve the gasdynamic equations in the form of decoupled compatibility relations. In the SCM technique the coefficient matrices are split according to the sign of their eigenvalues. The derivatives associated with each split-coefficient matrix are approximated by one-sided difference operators consistent with signal propagation paths. The results demonstrate that problems of conventional finite-difference methods with nonorthogonal grids are alleviated in the SCM approach. In addition, the solutions obtained using the SCM technique show that strong crossflow gradients, including crossflow shocks, can be accurately computed. To treat flows containing embedded streamwise shock waves the SCM technique is replaced, at grid points detected to be in the vicinity of a shock, by the monotonic self-adjusting hybrid/artificial compression method (ACM). The governing equations are cast in conservation law form in the shock-capturing ACM approach with damping terms added to eliminate postshock oscillations. Streamwise shocks of sufficient strength to cause conventional shock-capturing methods to fail are resolved using the combined SCM/ACM technique.

Introduction

THE split-coefficient matrix (SCM) method[1,2] is a new finite-difference scheme based on the theory of characteristics. In this paper an explicit SCM technique is developed for the computation of three-dimensional, inviscid, steady, supersonic flow. The technique is designed for the analysis of Earth and planetary re-entry vehicle flowfields and includes equilibrium real-gas capability. The required initial data plane is obtained using a recently developed three-dimensional, split-coefficient matrix, time-dependent, blunt-body code.[3]

The ideas underlying the SCM approach are not new; for example, Courant, Isaacson, and Rees[4] proposed using one-sided differencing consistent with the sign of the eigenvalues of the coefficient matrices. However, the concept was not widely adopted. One exception is the work of Gordon.[5] Based on the theoretical analysis of Anucina,[6] Gordon further developed the approach of diagonalizing the coefficient matrices and forming associated one-sided differences and applied the method to several time-dependent problems. Scala and Gordon[7] extended the approach to the solution of the time-dependent, two-dimensional Navier-Stokes equations. They derived a hyperbolic subsystem, split off from the viscous terms, and differenced this set according to the sign of the characteristics.

The recent renewal of interest in utilizing the theory of characteristics as a basis for constructing finite-difference methods was generated by Moretti's studies[8-10] and by the advent of flux-vector splitting algorithms.[11-13] Moretti developed the second-order λ-scheme and showed that it yielded improved accuracy, compared to conventional finite-difference methods, in a variety of applications. Results for steady supersonic flow demonstrate that the λ-scheme, although not a shock-capturing method, is able to resolve embedded crossflow shocks. The SCM approach differs somewhat from the λ-scheme, although both solve the primitive variable form of the governing equations. The differences and similarities of the SCM and λ-scheme approaches are described in Ref. 2. In essence, the use of matrix algebra to derive the SCM formulation avoids ambiguities that may arise with the λ-scheme in associating derivatives with characteristic propagation directions. The SCM approach has been identified[2] as the primitive variable counterpart of the conservation law flux-vector splitting approach. By not employing the conservation law form, the SCM approach needs no special treatment when the eigenvalues change sign. The blending terms and transition operators of the flux-vector approach are not required.

The steady supersonic SCM technique is formulated to correctly treat zones of supersonic crossflow. An embedded shock-fitting scheme is required to solve exactly the crossflow shock that terminates these zones. Fortunately, for most cases, the SCM technique can accurately resolve the crossflow discontinuity without invoking a shock-fitting scheme. However, embedded streamwise shocks are a source of numerical difficulty. One alternative to the complexities of an embedded shock-fitting approach is to solve the conservation law form of the governing equations. Conventional, explicit, second-order finite-difference solutions of the conservation law equations exhibit spurious postshock oscillations that grow with increasing shock strength. First-order methods produce smooth shock profiles, but if used throughout the flowfield require too many grid points for adequate resolution. Harten and Zwas[14] devised the monotonic self-adjusting hybrid algorithm to capture embedded shocks by reducing a second-order technique to first-order accuracy in the vicinity of a shock. The hybrid scheme is easily coupled to an existing second-order method and employs switches based

Presented as Paper 82-0287 at the AIAA 20th Aerospace Sciences Meeting, Orlando, Fla., Jan. 11-14, 1982; submitted Jan. 22, 1982; revision received Sept. 20, 1982. Copyright © American Institute of Aeronautics and Astronautics, Inc., 1982. All rights reserved.

*Research Engineer, Aerothermodynamics, Re-entry Systems Division. Member AIAA.
†Engineer, Thermodynamics Analysis, Re-entry Systems Division. Member AIAA.
‡Professor of Aerospace Engineering and Consultant, General Electric Re-entry Systems Division. Member AIAA.

on local flow gradients to add dissipation and yield a nonoscillatory shock profile. In contrast to locally first-order methods, the results presented by Minailos[15] illustrate the advantages of using higher order monotonic schemes. The artificial compression method (ACM) is a second-order monotonic algorithm developed by Harten[16] to sharpen the definition of embedded shock waves and improve overall solution accuracy. In this paper the ACM technique is applied in conjunction with the self-adjusting hybrid method and both are implemented through modifications of the basic explicit MacCormack algorithm.[17]

Review of the Baseline 3IS Technique

The split-coefficient matrix/locally monotonic scheme was developed within the framework of the GE three-dimensional, inviscid, supersonic 3IS flowfield code. The code contains options for asymmetric, pitch-plane symmetric, and axisymmetric flow. The axisymmetric option is labeled 2IS. The derivation of the 3IS algorithm is presented in detail in Ref. 18 which also includes a program listing. Comparisons to ground and flight test data have been used to validate the technique. The code has been applied in the design of a variety of re-entry vehicles and used extensively in post- and preflight analyses.

Several features of the baseline 3IS code are shared by the split-coefficient matrix version (3IS/SCM). The self-adjusting hybrid/artificial compression method (ACM), incorporated into the SCM version, also retains features of the 3IS technique. All versions employ the independent variables shown in Fig. 1a. A vertically offset cylindrical reference frame is chosen to allow computation of bent-axis configurations. A rectangular computational domain, bounded by the bow shock and body surfaces, is obtained by the independent variable transformation [see Appendix, Eq. (A1)]. The selected dependent variables (Fig. 1b) are the logarithm of pressure P, entropy S, and the velocity component ratios, $\sigma=u/w$ and $\tau=v/w$ where u, v, and w are the velocity components in the r, ϕ, and z directions, respectively. The 3IS code also contains an option to solve the governing equations cast in conservation law form. The ACM technique invokes this option at grid points neighboring embedded shocks.

In the 3IS code MacCormack's second-order, explicit, predictor-corrector algorithm[17] is used to solve the Euler gasdynamic equations. In vector-matrix form the governing equations are

$$d_Z+\underline{A}d_X+\underline{B}d_Y+c=0 \tag{1}$$

where $d^T=(P,\ \sigma,\ \tau,\ S)$. The coefficient matrices $\underline{A}$ and $\underline{B}$ are given in Eq. (A3) and the vector of source terms c is defined in Eq. (A4). The corresponding weak conservation law form of Eq. (1) is presented in Ref. 18. For axisymmetric flow the conservation law form of the governing equations reduces to

$$F_Z+G_X+R=0 \tag{2}$$

where

$$F=\frac{1}{X_r}\begin{bmatrix}\rho w\\ p+\rho w^2\\ \rho uw\end{bmatrix},\quad G=\frac{1}{X_r}\begin{bmatrix}\rho u\\ \rho uw\\ p+\rho u^2\end{bmatrix} \tag{3}$$

$$R=\frac{1}{rX_r}\begin{bmatrix}\rho u\\ \rho uw\\ \rho u^2\end{bmatrix}$$

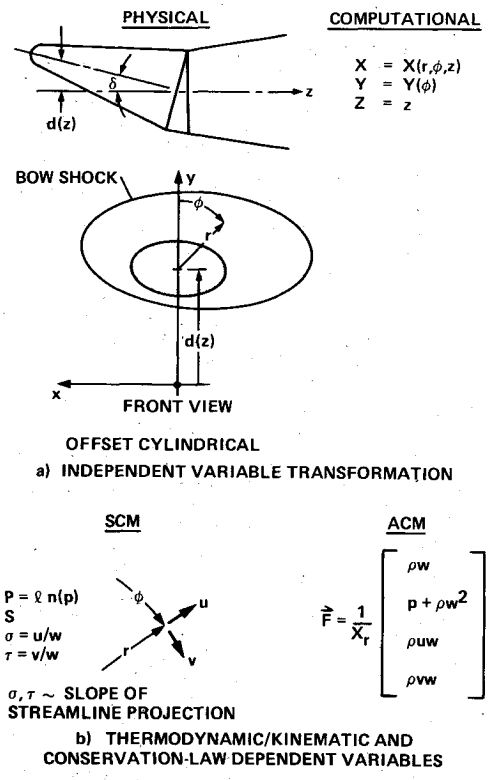

Fig. 1 Selection of variables for the split-coefficient matrix (SCM) method and the artificial compression method (ACM).

The bow shock is treated as a sharp discontinuity in the 3IS code. The same shock-fitting scheme is used in all versions of the code. The scheme proposed by Kentzer[19] combines the upwinding characteristic compatibility relation with the differentiated shock jump conditions. The propagation of the shock is implemented in a predictor-corrector algorithm following the approach of Moretti and Pandolfi.[20]

In the 3IS technique emphasis is placed on the numerical treatment of the body boundary. Surface pressure is obtained by iteratively solving the downrunning characteristic compatibility relation. Velocity components are determined from the inviscid flow tangency condition and the solution of a tangential momentum equation. This iterative method of characteristics boundary scheme, described in detail in Ref. 18, is retained as an option in the 3IS/SCM version.

Split-Coefficient Matrix (SCM) Formulation

The derivation of the split-coefficient matrix form of Eq. (1) is presented in the Appendix. The derivation follows a straightforward matrix algebra approach. However, the selection of σ and τ as dependent variables and the provision for a bent-axis leads to some algebraic complexity. In the SCM technique, Eq. (1) is replaced by

$$d_Z+\underline{A}_+d_{X_b}+\underline{A}_-d_{X_f}+\underline{B}_+d_{Y_b}+\underline{B}_-d_{Y_f}+c=0 \tag{4}$$

where the split matrices $\underline{A}_+$, $\underline{A}_-$, $\underline{B}_+$, and $\underline{B}_-$ are defined in Eqs. (A16) and (A18). The subscripts b and f designate approximations by one-sided backward and forward difference operators, respectively. MacCormack's predictor-corrector integration algorithm is retained in the SCM version of the 3IS code. To maintain second-order accuracy with one-sided differencing, three-point backward and two-point forward derivative approximations in the predictor step are followed by two-point backward and three-point forward approximations in the corrector step. An alternative integration algorithm proposed by Warming and Beam[21] and used in split form by Steger and Warming[13] and Daywitt[3] has also been

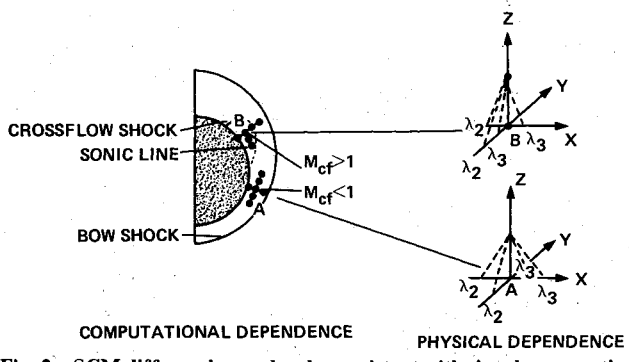

Fig. 2 SCM differencing molecule consistent with signal propagation paths.

added as an option in the 3IS/SCM code. This option requires additional storage and increases computational costs. However, the algorithm employs a symmetric computational molecule and thus eliminates problems that can arise due to the inherent asymmetry of the MacCormack scheme.

By solving Eq. (4) in lieu of Eq. (1), the SCM technique is more allied to a method of characteristics approach. As illustrated in Fig. 2, the value and sign of the projections of the characteristic slopes λ serve to weight the influence of each point in the finite-difference computational molecule. For example, in zones of supersonic crossflow, such as at point B in Fig. 2, the computational domain does not include points lying in the crossflow downstream direction, thus properly modeling signal propagation in supersonic flow.

To obtain a body boundary scheme consistent with the SCM algorithm at interior points, flow tangency is imposed and the differentiated tangency condition is used to replace the uprunning characteristic compatibility relation. The flow equations at the body surface are derived by first substituting Eq. (A18) into Eq. (A19) and postmultiplying by $\underline{S}^{-1}$ to yield

$$\underline{S}^{-1}d_Z+\underline{\Lambda}_A\underline{S}^{-1}d_X+\underline{S}^{-1}g=0 \tag{5}$$

where

$$g=\underline{T}\underline{\Lambda}_B\underline{T}^{-1}d_Y+c \tag{6}$$

The diagonal $\underline{\Lambda}$ matrices are defined in Eqs. (A10) and (A11). The coefficient matrices $\underline{S}$ and $\underline{T}$ are given in Eqs. (A13) and (A15), respectively. The flow tangency condition is $A=0$, where A is defined in Eq. (A5). The differentiated tangency condition is

$$A_Z=\sigma_Z-(r_{b_\phi}/r_b)\tau_Z-C \tag{7}$$

where

$$C=\tilde{\tau}\left(\frac{r_{b_{\phi z}}}{r_b}-\frac{r_{b_\phi}r_{b_z}}{r_b^2}\right)+r_{b_{zz}}+d''\left(\cos\phi+\frac{r_{b_\phi}}{r_b}\sin\phi\right) \tag{8}$$

with $\tilde{\tau}$ defined in Eq. (A6). At the body surface, Eq. (7) replaces the second row of Eq. (5) and with tangency imposed the system becomes

$$\underline{D}d_Z+e+f+C[0,-1,0,0]^T=0 \tag{9}$$

where $e=\underline{\Lambda}_A\underline{S}^{-1}d_X$ and $f=\underline{S}^{-1}g$, with the second element of e and f set equal to zero and

$$\underline{D}=\begin{bmatrix} d_{11} & d_{12} & d_{13} & 0 \\ 0 & 1 & d_{23} & 0 \\ d_{31} & d_{32} & d_{33} & 0 \\ 0 & 0 & 0 & 1 \end{bmatrix}$$

with

$$d_{11}=\frac{a^2}{\gamma w^2}$$

$$d_{12}=\left(\frac{X_\phi}{r}-\tau DX_r\right)\Big/\left(\tau X_r-\sigma\frac{X_\phi}{r}\right)$$

$$d_{13}=-(X_r-\sigma DX_r)\Big/\left(\tau X_r-\sigma\frac{X_\phi}{r}\right)$$

$$d_{23}=-\frac{r_{b_\phi}}{r_b},\qquad d_{31}=\frac{-a\beta}{\gamma(w^2-a^2)}$$

$$d_{32}=\alpha^2X_r,\qquad d_{33}=\alpha^2\frac{X_\phi}{r} \tag{10}$$

The terms α and D in Eq. (10) are defined in Eq. (A5) and the term β in Eq. (A12). After some rearrangement, the governing equations in the SCM body boundary scheme may be written in scalar form as

$$\tau_Z=\left\{\omega C+d_{31}\left[\left(\tau+\sigma\frac{r_{b_\phi}}{r_b}\right)d_{11}g_1-\left(\tau D+\frac{r_{b_\phi}}{r_b}\right)g_2-(1-\sigma D)g_3\right]-\left(\tau+\sigma\frac{r_{b_\phi}}{r_b}\right)d_{11}E\right\}\Big/\left(\eta-\omega\frac{r_{b_\phi}}{r_b}\right)$$

$$\sigma_Z=\frac{r_{b_\phi}}{r_b}\tau_Z+C$$

$$P_Z=-\left[\left(d_{32}\frac{r_{b_\phi}}{r_b}+d_{33}\right)\tau_Z+d_{32}C+E\right]\Big/d_{31}$$

$$S_Z=-BS_Y \tag{11}$$

where

$$\omega=-d_{31}\left(\tau D+\frac{r_{b_\phi}}{r_b}\right)-\left(\tau+\sigma\frac{r_{b_\phi}}{r_b}\right)d_{11}d_{32}$$

$$E=\lambda_3^A(d_{31}P_X+d_{32}\sigma_X+d_{33}\tau_X)+d_{31}g_1+d_{32}g_2+d_{33}g_3$$

$$\eta=-\frac{a^2}{\gamma(w^2-a^2)}\left[X_r\frac{r_{b_\phi}}{r_b}\left(\tau+\sigma\frac{r_{b_\phi}}{r_b}\right)+\frac{\beta}{a}(1-\sigma D)\right] \tag{12}$$

and λ_3^A is given in Eq. (A11). Because the body surface is a stream surface in inviscid flow the entropy equation contains only meridional Y derivatives. However, an entropy relaxation scheme such as described in Ref. 18 may be employed to allow the surface entropy to change from the initially prescribed blunt-body value.

The SCM body boundary scheme removes problems that occur when using the method of characteristics (MOC) body boundary scheme with nonorthogonal grids. At axial surface discontinuities the MOC scheme is superior due to its iterative corrector step and thus is retained as an option in the 3IS/SCM code.

Monotonic Shock-Capturing Method

Embedded streamwise shocks generated, for example, by conical flares or flap control surfaces may cause the conventional 3IS code to fail. Utilizing the option to solve the conservation law form of the governing equations may alleviate this problem. However, the computed flowfield will

contain nonphysical postshock oscillations. The weighted one-sided differencing in the SCM technique eliminates the shock oscillation problem for crossflow shocks that arise due to the deceleration of supersonic crossflow. The SCM differencing cannot, however, properly account for embedded streamwise discontinuities.

First-order, monotonic, shock-capturing schemes provide a mechanism to suppress oscillations but higher order schemes are generally required for re-entry flowfield analysis. Harten's[16] artificial compression method (ACM) achieves second-order accuracy but retains monotonic properties. The ACM technique is easily developed through modifications of the MacCormack algorithm and is thus an attractive alternative to the more complicated embedded shock-fitting approach.

The ACM algorithm, implemented in the axisymmetric 2IS code, is employed only at field points determined to be near a streamwise discontinuity. A simple shock detection scheme is used to locate points to be advanced by the ACM algorithm. The vehicle geometry is monitored to locate a shock generated by a body-slope discontinuity. The formation of a shock due to a coalescence of compression waves is detected by monitoring the pressure distribution across the shock layer. In the detection scheme devised by Moretti[22] a cubic polynomial is formed with pressure as the independent variable and the radial distance X as the dependent variable. A shock is assumed to have formed if $dX(P)/dP=0$. Once formed, the shock's motion through the field is tracked by scanning the radial pressure. If the shock strength decays sufficiently, the ACM algorithm is automatically replaced by the SCM technique.

The ACM technique solves the conservation law equations [Eq. (2)] in modified form. To formulate the ACM technique, the locally monotonic, first-order, self-adjusting hybrid scheme[14] is first developed by adding an artificial viscosity term to the MacCormack corrector step. The ACM scheme, which can be used only in conjunction with a first-order method, is then obtained by adding a so-called artificial compression flux term to the self-adjusting hybrid scheme solution. The ACM concept can be used with any first-order scheme. The first-order self-adjusting hybrid method was selected because it is easily obtained by modifying the MacCormack algorithm. The necessary modifications to the 2IS code are patterned after the procedure described by Sod.[23] Denoting the solution vector following the MacCormack corrector step as $F^{n\hat{+}1}$, the self-adjusting hybrid solution vector $F^{n\bar{+}1}$ is given by

$$F^{n\bar{+}1} = F^{n\hat{+}1} + \tfrac{1}{8}(\theta^n_{J+\frac{1}{2}}\Delta F^n - \theta^n_{J-\frac{1}{2}}\nabla F^n) \qquad (13)$$

where J is the radial direction grid index and $\theta=\theta(P)$ is a so-called switch. If $\theta=0$ the regular MacCormack scheme is obtained and if $\theta=1$ the resulting scheme is first-order accurate. The switches are a measure of the local pressure gradient with values ranging from 1 in shock regions to 0 in regions of smooth flow. The method used to compute θ is described in Ref. 23. The smoothed shock profiles resulting from the application of Eq. (13) are more sharply defined by the ACM algorithm given by

$$F^{n+1} = F^{n\bar{+}1} - \frac{\Delta Z}{2\Delta X}\delta(\theta^n Q^n) \qquad (14)$$

where $Q=Q(F)$ is the artificial compression flux vector. The scheme used to construct Q, based on differences of the solution vector at level n, is detailed in Ref. 23.

The ACM shock-capturing approach is not limited to axisymmetric problems. Extension to three-dimensional flow can be accomplished by devising a spatially split algorithm analogous to the time-split MacCormack scheme. The three-dimensional version is thus not as readily incorporated into an existing code.

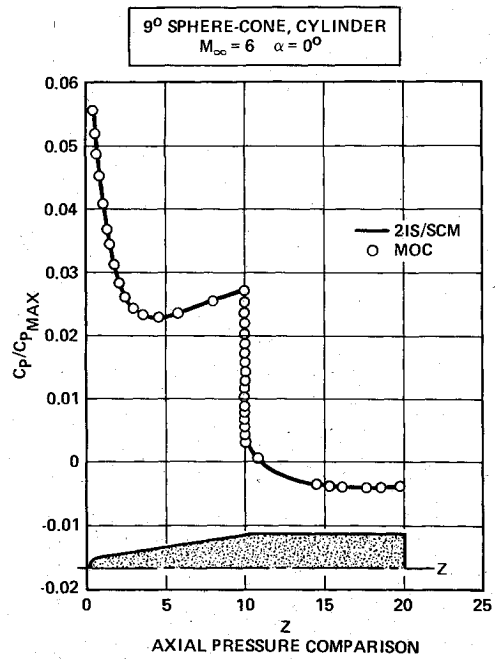

Fig. 3 SCM expansion test case: comparison with method of characteristics code that employs exact Prandtl-Meyer relations.

Results

The axisymmetric sphere-cone, cylinder configuration shown in Fig. 3 was chosen to validate and assess the split-coefficient matrix formulation. The selection of an axisymmetric flowfield test case enabled use of the GE method of characteristics (MOC) code[24] to compute benchmark comparison solutions. The GE-MOC code contains a provision for the exact Prandtl-Meyer expansion solution at the cone-cylinder juncture. Figure 3 shows that the SCM surface pressure results, labeled 2IS/SCM, agree precisely with the MOC solution, including the pressure level immediately following the turn onto the cylinder. This sphere-cone, cylinder configuration at $M_\infty=2$ was also used to assess the iterative MOC and SCM body boundary options in the 2IS/SCM code. For a coarse mesh ($\Delta X=0.1$), use of the iterative MOC body boundary scheme led to a slight deterioration of the solution. This mesh spacing dependence was removed with the use of the SCM body boundary scheme.

Figure 4 shows the results of a case used to validate the three-dimensional 3IS/SCM technique. The conventional 3IS code was employed to compute a comparison solution. The configuration, illustrated in Fig. 4a, is a candidate design for a Venus aerocapture mission. Analysis of this bent-axis, biconic vehicle requires application of the axis offset and real-gas features of the 3IS/SCM code. As shown by the axial pressure distribution in Fig. 4b, the 3IS/SCM code is able to resolve the sharp pressure jumps through the sequence of turns in the region joining the forward sphere-cone to the frustum. For this configuration and flow condition the 3IS/SCM results are in close agreement with the 3IS code predictions.

Figure 5a depicts a vehicle shape that was contrived to test the capability of the 3IS/SCM technique on a representative high lift-to-drag ratio configuration. The geometry of the spherically capped vehicle evolves through a sequence of elliptical cross sections, linked by straight line axial segments, to an elliptic cone with axis ratio $A/B=2$. The conventional 3IS code fails, as shown in Fig. 5a, shortly after reaching the elliptic cone segment. This failure may be attributed to the nonorthogonality of the circular cylindrical coordinate rays with the elliptic cone surface. In this case, the coordinate rays are inclined as much as 38 deg off of the desired surface normal direction. In contrast, the 3IS/SCM code encountered

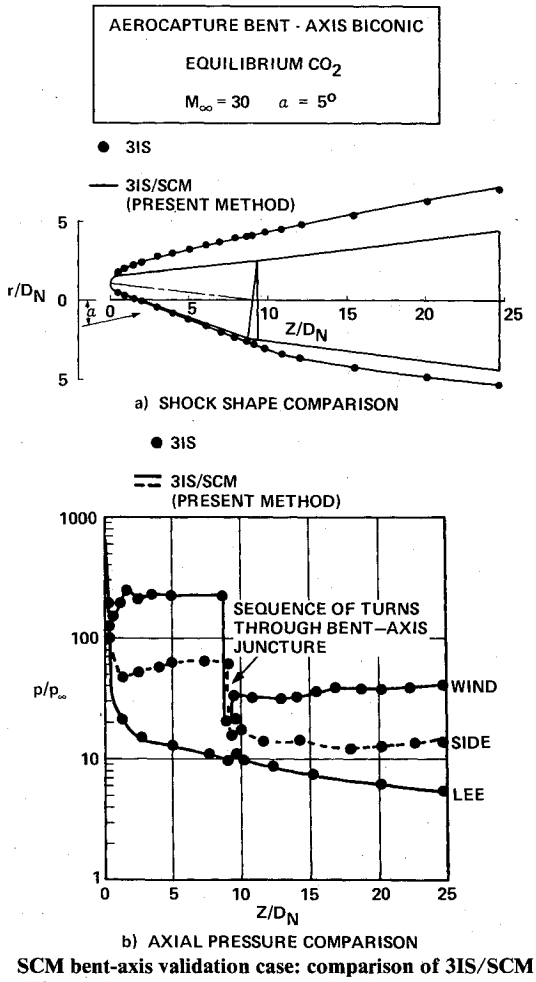

Fig. 4 SCM bent-axis validation case: comparison of 3IS/SCM with baseline 3IS code for aerocapture real-gas flowfield.

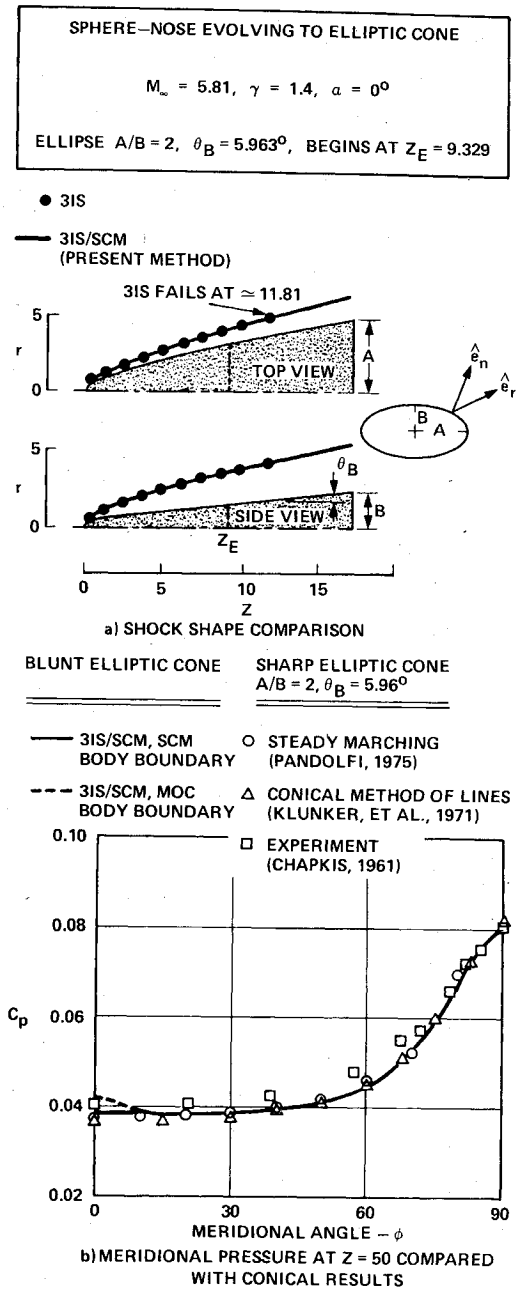

Fig. 5 Mesh skewness and strong crossflow gradient test case: baseline 3IS code fails.

no difficulties despite the mesh skewness and steep crossflow gradients that develop.

The 3IS/SCM computation of the flowfield about the blunt-nose configuration shown in Fig. 5a was extended to axial station $Z = 50$ to permit comparisons with sharp elliptic cone experimental data[25] and the results computed by Klunker et al.[26] and Pandolfi.[27] The comparison numerical methods are well suited to this problem. The inviscid method of lines technique developed in Ref. 26 is designed specifically for conical flow analyses. Pandolfi's method, described in Ref. 27, is a finite-difference marching technique tailored to elliptic cone computations. Pandolfi showed that accurate finite-difference solutions can be obtained by employing elliptical coordinates and using the ratio of contravariant velocity components as dependent variables. The experimental meridional pressure distribution and numerical results are shown in Fig. 5b. As indicated by the dashed line in Fig. 5b, the 3IS/SCM code employing the iterative MOC body boundary scheme evolved to the conical solution except for the anomalous rise in pressure near the $\phi = 0$ symmetry plane. This problem was removed, as shown by the solid line in Fig. 5b, with the use of the SCM body boundary scheme in the 3IS/SCM code.

To test the performance of the 3IS/SCM at high angle-of-attack supersonic crossflow conditions, the flowfield about a 4.7 deg sphere-cone at $M_\infty = 10$ and 15 deg angle of attack was computed. The formation of the leeside crossflow shock caused the conventional 3IS code to fail. Use of the iterative MOC body boundary scheme in the 3IS/SCM code led to erratic pressure oscillations near the crossflow shock as shown by the dashed line in Fig. 6. This behavior is to be expected since the iterative MOC scheme solves the downrunning, but not the meridional compatibility relations. The solid line shown in Fig. 6 demonstrates that the 3IS/SCM technique, with the SCM body boundary scheme, properly accounts for zones of subsonic and supersonic crossflow and establishes the crossflow shock between two grid points.

For the computation of axial or streamwise shocks, such as induced by flares or flap control surfaces, the SCM approach offers little advantage over conventional finite-difference methods. Because the flow component is typically subsonic in the radial r direction, the SCM algorithm applied at points in the vicinity of an embedded flare shock incorrectly employs points on both sides of the discontinuity. A mild flare compression test case is shown in Fig. 7. The iterative MOC body boundary scheme was selected for both the 2IS and 2IS/SCM computations. The comparison solution is obtained using the GE-MOC code with embedded shock-fitting employed at the 5 deg compression turn. The results shown in Fig. 7 indicate that for mild axial-type compressions the SCM formulation yields a more accurate solution than the conventional 2IS code. However, as shown in Fig. 8a, for a

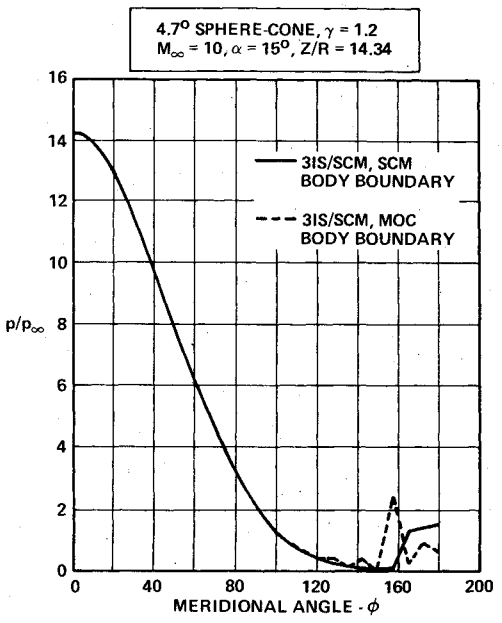

Fig. 6 Crossflow shock test case: comparison of body boundary schemes in 3IS/SCM code.

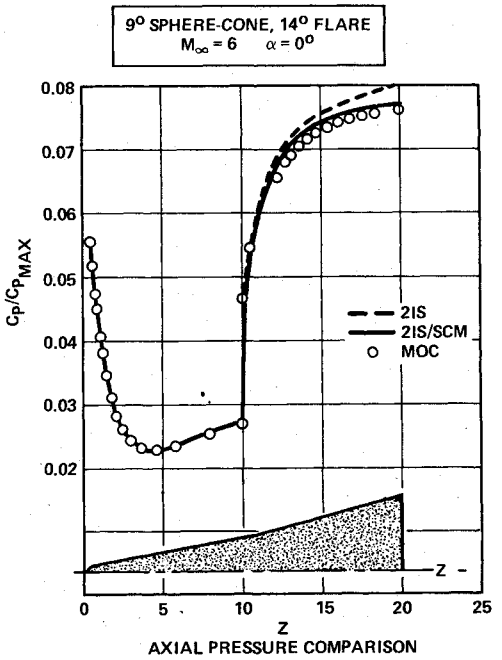

Fig. 7 SCM 5 deg compression test case: comparison with baseline 2IS code and shock-fitting method of characteristics code.

stronger embedded flare shock both the 2IS and 2IS/SCM codes fail to match the MOC results.

The self-adjusting hybrid/artificial compression method (ACM), developed to treat axial-type embedded shock waves, was applied to compute the 15 deg compression test case shown in Fig. 8. The ACM results match the MOC solution. The shock detection algorithm, used to locate points to be advanced by the ACM technique, tracked the flare shock to its intersection with the bow shock. In this case, the embedded shock strikes the bow shock resulting in a type VI shock interaction.[28] The postinteraction flowfield consists of a kinked bow shock, an embedded contact surface, and an expansion fan that strikes the body surface. The surface pressure distribution obtained by the MOC code and the 2IS/SCM code with the ACM technique (Fig. 8a) clearly show the expansion fan reaching the surface of the flare. With the

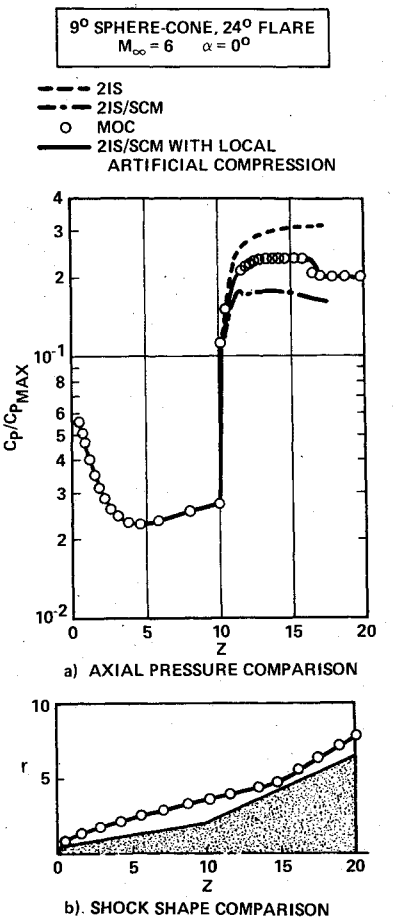

Fig. 8 SCM/ACM 15 deg compression test case: comparison with shock-fitting method of characteristics code (baseline 2IS and 2IS/SCM codes fail).

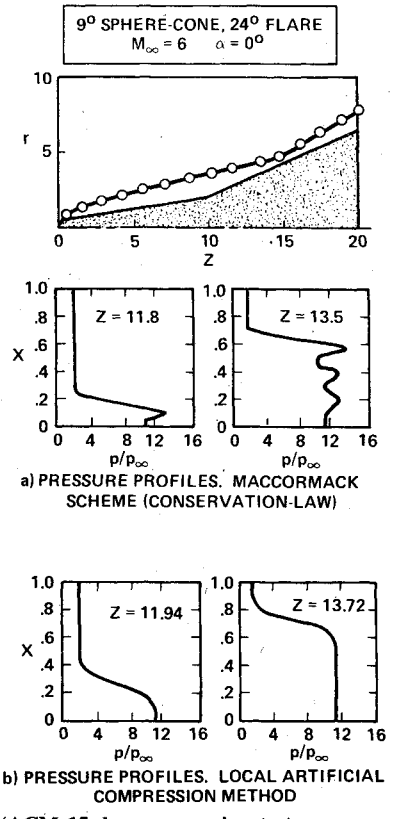

Fig. 9 SCM/ACM 15 deg compression test case: comparison with conservation law form of 2IS code.

disappearance of the embedded shock aft of the shock-shock intersection, the shock detection algorithm automatically terminates ACM computations. The SCM technique, employed at all points except those neighboring the embedded shock, is formulated to capture the contact surface discontinuity. This feature of the SCM technique is a result of the choice of dependent variables and the differencing algorithm. In this compression test case, the contact surface is too weak to be discerned in the shock-layer density profiles.

In Fig. 9 pressure distributions through the shock layer, aft of the 15 deg compression turn, are presented. Results obtained using an option in the 2IS code to solve the governing equations in conservation law form are shown in Fig. 9a. Although the surface pressure in Fig. 9a is not greatly in error, the pressure profiles through the shock layer display large postshock oscillations. The substantially improved solution yielded by the 2IS/SCM technique, with ACM employed in the vicinity of the shock, is evident in Fig. 9b.

Conclusions

The development of the split-coefficient matrix technique to solve the steady supersonic gasdynamic equations was found to be algebraically more complex and more complicated to program than conventional finite-difference methods. However, the matrix algebra approach is straightforward and the resulting decoupled compatibility relations and differencing algorithm closely model the hyperbolic nature of the flow. An SCM body boundary scheme was developed and shown to be superior in certain cases to an iterative method of characteristics approach. Results demonstrate that the SCM technique, compared to a conventional finite-difference method, is less sensitive to grid nonorthogonality and alleviates problems in resolving crossflow shocks.

A locally monotonic shock-capturing technique was adopted to treat streamwise embedded shocks. The technique is employed only at points detected to be in the vicinity of a shock discontinuity. To validate this technique the flowfield about a flared vehicle was computed. The embedded flare shock was of sufficient strength to preclude use of the primitive variable formulation in the conventional finite-difference technique. The results presented show the improved accuracy of the split-coefficient matrix/locally monotonic scheme compared to the conservation law shock-capturing approach.

Appendix: Split-Coefficient Matrix (SCM) Form of the Governing Equations

For the computation of steady, supersonic, inviscid flow an offset cylindrical coordinate reference frame (r,ϕ,z) is chosen. As shown in Fig. 1a, $d(z)$ is the vertical offset of the cylindrical origin from the reference z axis. This offset facilitates the computation of bent-axis vehicles but complicates the form of the governing equations. The independent variable transformation

$$X=\frac{r-r_b(\phi,z)}{r_s(\phi,z)-r_b(\phi,z)}$$

$$Y=G(\phi)=\pi-\tan^{-1}\left(\frac{1}{K}\tan\phi\right), \quad (1\le K<\infty)$$

$$Z=z \tag{A1}$$

maps the shock layer into a rectangular computational domain. In Eq. (A1) the subscripts b and s refer to the body and shock surfaces, respectively, and K is a meridional mesh clustering parameter.

The selected dependent variables are the logarithm of pressure P, entropy S, and the velocity ratios, $\sigma=u/w$ and $\tau=v/w$. As shown in Fig. 1b, u, v, and w are the velocity components in the r, ϕ, and z directions, respectively. In the transformed computational domain, the steady Euler gasdynamic equations in vector-matrix form are

$$d_Z+\underline{A}d_X+\underline{B}d_Y+c=0 \tag{A2}$$

where $d^T=(P,\ \sigma,\ \tau,\ S)$ is the vector of dependent variables. The rows in Eq. (A2) correspond in order to the continuity, X and Y momentum, and energy equations. The coefficient matrices are

$$\underline{A}=\begin{bmatrix} \alpha^2\left(A-\frac{a^2}{w^2}DX_r\right) & \gamma\alpha^2X_r & \gamma\alpha^2\frac{X_\phi}{r} & 0 \\ \frac{a^2}{\gamma w^2}(X_r+\sigma\alpha^2\kappa) & A+\frac{a^2}{w^2}\sigma\alpha^2X_r & \frac{a^2}{w^2}\sigma\alpha^2\frac{X_\phi}{r} & 0 \\ \frac{a^2}{\gamma w^2}\left(\frac{X_\phi}{r}+\tau\alpha^2\kappa\right) & \frac{a^2}{w^2}\tau\alpha^2X_r & A+\frac{a^2}{w^2}\tau\alpha^2\frac{X_\phi}{r} & 0 \\ 0 & 0 & 0 & A \end{bmatrix} \tag{A3}$$

$$\underline{B}=\begin{bmatrix} \alpha^2\left(B-\frac{a^2}{w^2}d'\frac{Y_\phi}{r}\sin\phi\right) & 0 & \alpha^2\gamma\frac{Y_\phi}{r} & 0 \\ \frac{a^2}{\gamma w^2}\sigma\alpha^2\left(B-d'\frac{Y_\phi}{r}\sin\phi\right) & B & \frac{a^2}{w^2}\sigma\alpha^2\frac{Y_\phi}{r} & 0 \\ \frac{a^2}{\gamma w^2}\frac{Y_\phi}{r}(1+\tau^2\alpha^2) & 0 & B+\alpha^2\frac{a^2}{w^2}\tau\frac{Y_\phi}{r} & 0 \\ 0 & 0 & 0 & B \end{bmatrix}$$

and the vector of source terms is

$$c=\begin{bmatrix} \alpha^2\dfrac{\sigma\gamma}{r} \\ \dfrac{a^2\sigma^2\alpha^2}{w^2 r}-\dfrac{\tau\tilde{\tau}}{r} \\ \dfrac{\sigma\tilde{\tau}}{r}+\dfrac{a^2}{w^2}\alpha^2\tau\dfrac{\sigma}{r} \\ 0 \end{bmatrix} \tag{A4}$$

In the above expressions a is the local speed of sound and

$$\alpha^2=\frac{w^2}{w^2-a^2}, \quad \kappa=\sigma X_r+\tau\frac{X_\phi}{r}$$

$$A=\tilde{\sigma}X_r+\tilde{\tau}\frac{X_\phi}{r}+X_z, \quad B=\tilde{\tau}\frac{Y_\phi}{r}$$

$$D=\frac{1}{X_r}\left(X_z-d'X_r\cos\phi+d'X_\phi\frac{\sin\phi}{r}\right) \tag{A5}$$

with

$$\tilde{\sigma}=\sigma-d'\cos\phi, \qquad \tilde{\tau}=\tau+d'\sin\phi \tag{A6}$$

where the offset axis slope is given by

$$d'=\frac{\mathrm{d}[d(z)]}{\mathrm{d}z} \tag{A7}$$

The isentropic exponent

$$\gamma=\frac{\partial P}{\partial(\ell n\rho)}\bigg|_S=\gamma(P,S) \tag{A8}$$

is supplied in tabular or curve-fit form for specified gases in thermodynamic equilibrium.

Prior to adopting the SCM technique, the solution of the flowfield involved discretization of the governing equations in the form given by Eq. (A2). A better representation of the hyperbolic nature of the flow is obtained by recasting Eq. (A2) into the SCM form which, together with the appropriate one-sided derivative approximations, utilizes information contained in the characteristic compatibility relations. The general theory and derivation of the SCM form of the Euler equations for several sets of dependent and independent variables may be found in Refs. 1 and 2. The SCM form of the three-dimensional, unsteady Euler equations used to compute the flowfield about blunt nose tips is presented in Ref. 3. We derive below an SCM form appropriate for steady, three-dimensional, inviscid, supersonic flow. The SCM blunt-body technique described in Ref. 3 is used to generate the required initial data plane.

Because Eq. (A2) is hyperbolic, there exists a similarity transformation such that

$$\underline{A}=\underline{S}\underline{\Lambda}_A\underline{S}^{-1}, \qquad \underline{B}=\underline{T}\underline{\Lambda}_B\underline{T}^{-1} \tag{A9}$$

where $\underline{\Lambda}_A$ and $\underline{\Lambda}_B$ are diagonal matrices

$$\underline{\Lambda}_A=\mathrm{Diag}(\lambda_1^A,\lambda_2^A,\lambda_3^A,\lambda_1^A), \quad \underline{\Lambda}_B=\mathrm{Diag}(\lambda_1^B,\lambda_2^B,\lambda_3^B,\lambda_1^B) \tag{A10}$$

whose elements are the eigenvalues of the $\underline{A}$ and $\underline{B}$ coefficient matrices. The eigenvalues $\lambda_1^A=A$ and $\lambda_1^B=B$ are the slopes of the stream surface projected onto the X-Z and Y-Z planes, respectively. The corresponding slopes of the projection of the wave surface are

$$\lambda_{2,3}^A=\frac{w^2A-a^2DX_r\pm a\beta}{w^2-a^2}$$

$$\lambda_{2,3}^B=\frac{w^2B-a^2d'(Y_\phi/r)\sin\phi\pm a\Omega}{w^2-a^2} \tag{A11}$$

where

$$\beta=\sqrt{(w^2-a^2)(X_r^2+X_\phi^2/r^2)+w^2\kappa^2}$$

$$\Omega=Y_\phi/r\sqrt{w^2(\tau^2+1)-a^2} \tag{A12}$$

In Eq. (A9), $\underline{S}^{-1}$ and $\underline{T}^{-1}$ are matrices whose rows are the left eigenvectors of $\underline{A}$ and $\underline{B}$, respectively. The particular forms of $\underline{S}^{-1}$ and $\underline{T}^{-1}$ are not unique. Therefore, nonzero multiples of an eigenvector may be employed to simplify the algebra and assure that no indeterminate forms will appear. Once $\underline{S}^{-1}$ and $\underline{T}^{-1}$ are constructed it is necessary to determine the inverse of each. A suitable choice of eigenvectors leads to the result

$$\underline{S}=\begin{bmatrix} 0 & s_{12} & s_{13} & 0 \\ s_{21} & s_{22} & s_{23} & 0 \\ s_{31} & s_{32} & s_{33} & 0 \\ 0 & 0 & 0 & 1 \end{bmatrix}$$

with

$$s_{12}=\frac{\gamma(w^2-a^2)}{2a\beta}$$

$$s_{13}=-s_{12}$$

$$s_{21}=\frac{X_\phi}{r}\frac{\xi}{\psi}$$

$$s_{22}=-\frac{1}{2\beta\alpha^2\psi}\left[\frac{a\xi X_\phi}{r}-\beta(X_r+\sigma\kappa)\right]$$

$$s_{23}=\frac{1}{2\beta\alpha^2\psi}\left[\frac{a\xi X_\phi}{r}+\beta(X_r+\sigma\kappa)\right]$$

$$s_{31}=-X_r\frac{\xi}{\psi}$$

$$s_{32}=\frac{1}{2\beta\alpha^2\psi}\left[a\xi X_r+\beta\left(\frac{X_\phi}{r}+\tau\kappa\right)\right]$$

$$s_{33}=-\frac{1}{2\beta\alpha^2\psi}\left[a\xi X_r-\beta\left(\frac{X_\phi}{r}+\tau\kappa\right)\right] \tag{A13}$$

where

$$\xi=\tau X_r-\sigma\frac{X_\phi}{r}$$

$$\psi=X_r^2+\frac{X_\phi^2}{r^2}+\left(\tau\frac{X_\phi}{r}+\sigma X_r\right)^2 \tag{A14}$$

and

$$\underline{T}=\begin{bmatrix} 0 & t_{12} & t_{13} & 0 \\ t_{21} & t_{22} & t_{23} & 0 \\ 0 & \tfrac{1}{2} & \tfrac{1}{2} & 0 \\ 0 & 0 & 0 & 1 \end{bmatrix}$$

with

$$t_{12}=\frac{\gamma w^2 Y_\phi}{2a\Omega r}$$

$$t_{13}=-t_{12}$$

$$t_{21}=\frac{\sigma a^2}{\gamma w^2}$$

$$t_{22}=\left[\frac{\sigma}{2(1+\tau^2)}\right]\left(\tau+\frac{aY_\phi}{\Omega r}\right)$$

$$t_{23}=\left[\frac{\sigma}{2(1+\tau^2)}\right]\left(\tau-\frac{aY_\phi}{\Omega r}\right) \qquad \text{(A15)}$$

Substituting for the matrices on the right-hand side of Eq. (A9) and expanding on the matrix product yields

$$\underline{A}=\begin{bmatrix} \frac{1}{2}(\lambda_2^A+\lambda_3^A) & \alpha^2 X_r s_{12}(\lambda_2^A-\lambda_3^A) & \alpha^2\frac{X_\phi}{r}s_{12}(\lambda_2^A-\lambda_3^A) & 0 \\ \frac{s_{21}a^2\lambda_1^A}{w^2\gamma}+\frac{s_{22}\lambda_2^A-s_{23}\lambda_3^A}{2s_{12}} & \frac{X_\phi\lambda_1^A}{r\psi}\left(\frac{X_\phi}{r}+\tau\kappa\right)+\alpha^2X_r(s_{22}\lambda_2^A+s_{23}\lambda_3^A) & \frac{-X_\phi\lambda_1^A}{r\psi}(X_r+\sigma\kappa)+\alpha^2\frac{X_\phi}{r}(s_{22}\lambda_2^A+S_{23}\lambda_3^A) & 0 \\ \frac{s_{31}a^2\lambda_1^A}{w^2\gamma}+\frac{s_{32}\lambda_2^A-s_{33}\lambda_3^A}{2s_{12}} & \frac{-X_r\lambda_1^A}{\psi}\left(\frac{X_\phi}{r}+\tau\kappa\right)+\alpha^2X_r(s_{32}\lambda_2^A+s_{33}\lambda_3^A) & \frac{X_r\lambda_1^A}{\psi}(X_r+\sigma\kappa)+\alpha^2\frac{X_\phi}{r}(s_{32}\lambda_2^A+s_{33}\lambda_3^A) & 0 \\ 0 & 0 & 0 & \lambda_1^A \end{bmatrix}$$

$$\underline{B}=\begin{bmatrix} \frac{1}{2}(\lambda_2^B+\lambda_3^B) & 0 & t_{13}(\lambda_3^B-\lambda_2^B) & 0 \\ \frac{-t_{21}\lambda_1^B}{1+\tau^2}+\frac{1}{2t_{12}}(t_{22}\lambda_2^B-t_{23}\lambda_3^B) & \lambda_1^B & \frac{-\sigma\tau\lambda_1^B}{1+\tau^2}+t_{22}\lambda_2^B+t_{23}\lambda_3^B & 0 \\ \frac{1}{4t_{12}}(\lambda_2^B-\lambda_3^B) & 0 & \frac{1}{2}(\lambda_2^B+\lambda_3^B) & 0 \\ 0 & 0 & 0 & \lambda_1^B \end{bmatrix} \qquad \text{(A16)}$$

With the coefficient matrices expressed in terms of eigenvalues, a numerical method can be constructed to exploit the property that the flow at a point is determined by information transmitted along characteristic directions. The separate contributions associated with the positive and negative eigenvalues can be distinguished by considering the diagonal $\underline{\Lambda}$ matrices as being composed of two parts

$$\underline{\Lambda}=\underline{\Lambda}_+ +\underline{\Lambda}_- \qquad \text{(A17)}$$

where $\underline{\Lambda}_+$ contains only those eigenvalues $\lambda>0$, while $\underline{\Lambda}_-$ contains only negative eigenvalues. Because each term in all of the nonzero elements of the coefficient matrices [Eq. (A16)] is a linear combination of the eigenvalues, the coefficient matrices may be split according to the sign of the eigenvalues as

$$\underline{A}=\underline{S}\underline{\Lambda}_{A+}\underline{S}^{-1}+\underline{S}\underline{\Lambda}_{A-}\underline{S}^{-1}=\underline{A}_+ +\underline{A}_-$$

$$\underline{B}=\underline{T}\underline{\Lambda}_{B+}\underline{T}^{-1}+\underline{T}\underline{\Lambda}_{B-}\underline{T}^{-1}=\underline{B}_+ +\underline{B}_- \qquad \text{(A18)}$$

To match the correct signal propagation paths, the derivatives that are multiplied by the split-coefficient matrices must be approximated by appropriate one-sided difference operators. Backward differences are multiplied by the positive eigenvalue matrices while forward differences are associated with negative eigenvalues. Thus, in contrast to Eq. (A2), in the SCM method the finite-difference algorithm is used to solve the governing equations in the form

$$d_Z+\underline{A}_+ d_{X_b}+\underline{A}_- d_{X_f}+\underline{B}_+ d_{Y_b}+\underline{B}_- d_{Y_f}+c=0 \qquad \text{(A19)}$$

where the subscripts b and f designate approximations by one-sided backward and forward difference operators, respectively.

Acknowledgments

The authors wish to acknowledge the contributions made by Marijean Wade to this investigation. These include organizing the various program versions and data files and running the numerous cases involved in this study. This work was sponsored in part by the General Electric Company Independent Research and Development Program and in part by the Air Force Ballistic Missile Office under Contract F04701-78-C-0104.

References

[1] Chakravarthy, S. R., "The Split Coefficient Matrix Method for Hyperbolic Systems of Gasdynamic Equations," Ph.D. Dissertation, Dept. of Aerospace Engineering, Iowa State University, Ames, 1979.

[2] Chakravarthy, S. R., Anderson, D. A., and Salas, M. D., "The Split Coefficient Matrix Method for Hyperbolic Systems of Gasdynamic Equations," AIAA Paper 80-0268, Jan. 1980.

[3] Daywitt, J. E., "Improvements in Techniques for Computing Supersonic Blunt-Body Flows," AIAA Paper 81-0115, Jan. 1981.

[4] Courant, R., Isaacson, E., and Rees, M., "On the Solution of Nonlinear Hyperbolic Differential Equations by Finite-Differences," *Communications on Pure and Applied Mathematics*, Vol. 5, 1952, pp. 243-255.

[5] Gordon, P., "The Diagonal Form of Quasi-Linear Hyperbolic Systems as a Basis for Difference Equations," General Electric Company, Final Report, Naval Ordnance Laboratory Contract N60921-7164, Dec. 1969, pp. II.D-1-II.D-22.

[6] Anucina, N. N., "Difference Schemes for Solving the Cauchy Problem for Symmetric Hyperbolic Systems," *Soviet Mathematics—Doklady*, Vol. 5, 1964, pp. 60-64.

[7] Scala, S. M. and Gordon, P., "Solution of the Time-Dependent Navier-Stokes Equations for the Flow of Dissociating Gas over a

Circular Cylinder," *Fluid Physics of Hypersonic Wakes*, AGARD Conference Proceedings, No. 19, Vol. 1, May 1967.

[8] Moretti, G., "An Old Integration Scheme for Compressible Flows Revisted, Refurbished, and Put to Work," Polytechnic Institute of New York, Brooklyn, POLY M/AE Rept. 78-22, Sept. 1978.

[9] Moretti, G., "The λ-Scheme," *Computers and Fluids*, Vol. 7, Sept. 1979, pp. 191-205.

[10] Moretti, G., "Numerical Integration of Compressible, Viscous Flow Equations," Polytechnic Institute of New York, Brooklyn, POLY M/AE Rept. 79-40, Sept. 1979.

[11] Warming, R. F. and Beam, R. M., "On the Construction and Application of Implicit Factored Schemes for Conservation Laws," *SIAM-AMS Proceedings, Symposium on Computational Fluid Dynamics*, Vol. 11, 1978, pp. 85-97.

[12] Steger, J. L., "Coefficient-Matrices for Implicit Finite Difference Solution of the Inviscid Fluid Conservation-Law Equations," *Computer Methods in Applied Mechanics and Engineering*, Vol. 13, Feb. 1978, pp. 175-188.

[13] Steger, J. L. and Warming, R. F., "Flux Vector Splitting of the Inviscid Gasdynamic Equations with Applications to Finite Difference Methods," *Journal of Computational Physics*, Vol. 40, April 1981, pp. 263-293.

[14] Harten, A. and Zwas, G., "Self-Adjusting Hybrid Schemes for Shock Computations," *Journal of Computational Physics*, Vol. 9, June 1972, pp. 568-583.

[15] Minailos, A. N., "Significance of the Monotonicity of Finite-Difference Schemes in Shock-Capturing Methods," *USSR Computational Mathematics and Mathematical Physics*, Vol. 17, No. 4, 1977 (published Sept. 1978), pp. 235-240.

[16] Harten, A., "The Artificial Compression Method for Computation of Shocks and Contact Discontinuities, III: Self-Adjusting Hybrid Schemes," *Mathematics of Computation*, Vol. 32, April 1978, pp. 363-389.

[17] MacCormack, R. W., "The Effect of Viscosity in Hypervelocity Impact Cratering," AIAA Paper 69-354, April 1969.

[18] Daywitt, J., Brant, D., and Bosworth, F., "Computational Technique for Three-Dimensional Inviscid Flow Fields About Reentry Vehicles," SAMSO TR-79-5, April 1978.

[19] Kentzer, C. P., "Discretization of Boundary Conditions on Moving Discontinuities," *Proceedings of the Second International Conference on Numerical Methods in Fluid Dynamics, Lecture Notes in Physics*, Vol. 8, edited by M. Holt, 1970, pp. 108-113.

[20] Moretti, G. and Pandolfi, M., "Entropy Layers," *Computers and Fluids*, Vol. 1, Jan. 1973, pp. 19-35.

[21] Warming, R. F. and Beam, R. M., "Upwind Second-Order Difference Schemes and Applications in Aerodynamic Flows," *AIAA Journal*, Vol. 14, Sept. 1976, pp. 1241-1249.

[22] Moretti, G., "Thoughts and Afterthoughts About Shock Computations," Polytechnic Institute of Brooklyn, New York, PIBAL Rept. 72-37, Dec. 1972.

[23] Sod, G. A., "A Survey of Several Finite Difference Methods for Systems of Nonlinear Hyberbolic Conservation Laws," *Journal of Computational Physics*, Vol. 27, April 1978, pp. 1-31.

[24] Davis, R. S., "Analysis and Programming of Supersonic Field with Shock Intersection," General Electric Company, Philadelphia, Rept. GE-TIS-62SD105, April 1962.

[25] Chapkis, R. L., "Hypersonic Flow over an Elliptic Cone: Theory and Experiment," *Journal of the Aerospace Sciences*, Vol. 28, Nov. 1961, pp. 844-854.

[26] Klunker, E. B., South, J. C. Jr., and Davis, R. M., "Calculation of Nonlinear Conical Flows by the Method of Lines," NASA TR R-374, Oct. 1971.

[27] Pandolfi, M., "Supersonic Flow About Elliptic Cones with Large Semiaxis Ratio," Istituto DiMacchine E Motori Per Aeromobili, Torino, Italy, Rept. PP 172, Dec. 1975.

[28] Edney, B. E., "Anomalous Heat Transfer and Pressure Distributions on Blunt Bodies at Hypersonic Speeds in the Presence of an Impinging Shock," Aeronautical Research Institute of Sweden, FFA Rept. 115, Feb. 1968.

From the AIAA Progress in Astronautics and Aeronautics Series . . .

TRANSONIC AERODYNAMICS—v. 81

Edited by David Nixon, Nielsen Engineering & Research, Inc.

Forty years ago in the early 1940s the advent of high-performance military aircraft that could reach transonic speeds in a dive led to a concentration of research effort, experimental and theoretical, in transonic flow. For a variety of reasons, fundamental progress was slow until the availability of large computers in the late 1960s initiated the present resurgence of interest in the topic. Since that time, prediction methods have developed rapidly and, together with the impetus given by the fuel shortage and the high cost of fuel to the evolution of energy-efficient aircraft, have led to major advances in the understanding of the physical nature of transonic flow. In spite of this growth in knowledge, no book has appeared that treats the advances of the past decade, even in the limited field of steady-state flows. A major feature of the present book is the balance in presentation between theory and numerical analyses on the one hand and the case studies of application to practical aerodynamic design problems in the aviation industry on the other.

696 pp., 6×9, illus., $30.00 Mem., $55.00 List

TO ORDER WRITE: Publications Dept., AIAA, 1290 Avenue of the Americas, New York, N. Y. 10019